Electron diffraction study of small bundles of single-wall carbon nanotubes with unique helicity

J.-F. Colomer,[1,*] L. Henrard,[2] Ph. Lambin,[2] and G. Van Tendeloo[1]
[1]*EMAT, University of Antwerp (RUCA), Gronenborgerlaan 171, 2020 Antwerp, Belgium*
[2]*Laboratoire de Physique du Solide, FUNDP, 61 rue de Bruxelles, 5000 Namur, Belgium*
(Received 5 March 2001; revised manuscript received 26 April 2001; published 11 September 2001)

The selected-area electron diffraction technique has been used to investigate the structure of bundles of single-wall carbon nanotubes synthesized by the catalytic chemical vapor deposition method. The helicity and lattice packing of the single-wall carbon nanotubes within the bundles have been deduced from the experimental diffraction patterns on the basis of the geometry of the reciprocal space of carbon nanotubes and computer simulations based on the kinematical theory. We show that a precise helicity can be found within a given small bundle. We attribute this selectivity to the small number of nanotubes (20–30) in the bundles.

DOI: 10.1103/PhysRevB.64.125425 PACS number(s): 61.14.−x, 68.37.Lp, 61.46.+w

I. INTRODUCTION

Since their discovery in 1991,[1] carbon nanotubes have been the subject of an intensive research due to their extraordinary mechanical[2] and electronic[3,4] properties. Moreover, the intrinsic simplicity of the single-wall carbon nanotubes made them ideal objects for the investigation of reduced-dimensionality effects. Indeed, a single-wall carbon nanotube (SWNT) can be built by rolling up a single graphene sheet and is uniquely defined by its chiral vector $\mathbf{C}_{n,m}=n\mathbf{a}+m\mathbf{b}$, where **a** and **b** are the unit vectors of the honeycomb network, and n and m are integers.[5] Depending on the wrapping indices (n,m), different types of nanotubes are obtained: (1) zigzag nanotubes correspond to $(n,0)$ and have a chiral angle of 0°, (2) (n,n) armchair nanotubes have a chiral angle of 30°, and (3) other, chiral (n,m) nanotubes have a chiral angle ranging from 0° to 30°. The properties of a SWNT are determined by its diameter and chiral angle (helicity), which are uniquely defined by the couple (n,m). For example, a SWNT can behave either as a metal or a semiconductor depending on these two parameters.[6]

Due to recent progress in the production techniques, the SWNT's can now be synthesized in large quantities with high yields. For example, the SWNT's are commonly produced by the laser ablation method[7] and the electric arc discharge technique.[8] More recently, large-scale production of SWNT's by the catalytic chemical vapor deposition (CCVD) method has been reported.[9] The SWNT's synthesized by the first two methods have been intensively studied by many characterization techniques. Among these, high-resolution transmission electron microscopy (HRTEM) and x-ray diffraction have revealed the structure and morphology of the SWNT samples.[7,8] It appeared that the SWNT's are close packed in bundles and form a triangular lattice with a period of 17 Å. Assuming an intertube distance of 3.2 Å, it was concluded[7] that the mean tube diameter was 13.8 Å. Subsequent studies with Raman spectroscopy[11,12] and x-ray and neutron diffraction[13] showed that the tube diameter and the lattice parameter can vary inside the same sample. Different authors reported also that the atomic structure of the SWNT's depends on the growth conditions and on the production technique used.[14–17] Another, powerful technique for a direct determination of the helicity of the nanotubes is electron diffraction (ED), as first demonstrated for multiwall carbon nanotubes by Iijima *et al.*[10] Two complementary methods exist for the interpretation of the diffraction pattern produced by the carbon nanotubes. The reciprocal-space geometrical model[18–20] provides a qualitative understanding of the position and shape of the $hk.0$ reflections of a given carbon nanotube, and the kinematical theory of diffraction[21–25] makes it possible to calculate the positions and intensities of the spots in the diffraction pattern.

Experimentally, the first ED results on SWNT's have been obtained on samples produced by the double-laser ablation method.[24,26–29,31,32] Different conclusions have been drawn concerning the helicity of the tubes forming the bundles. Using nanodiffraction, Cowley *et al.*[26] found a predominant helicity corresponding to the armchair (10,10) nanotubes, together with a small proportion of (11,9) and (12,8) tubes. With the same type of sample, other nanodiffraction experiments did not reveal a predominant helicity, but only a weak preference for the armchair geometry.[27,28] Using selected-area electron diffraction (SAED), Bernaerts *et al.*[24] came to the conclusion that a bundle mixed several tube helicities. From these published observations, we conclude that the SWNT bundles produced by laser ablation present some distribution of tube helicities except for a few cases where a unique helicity has been found.[27,28,31] As for the SWNT's synthesized by electric arc discharge, detailed SAED experiments indicated an uniform distribution of helicity in the bundles.[25]

In this paper, we analyze electron diffraction data we have obtained on isolated, straight, and small bundles of single-wall carbon nanotubes produced by the CCVD method. We also performed diffraction experiments on SWNT samples produced by electric arc discharge for the sake of comparison. Our data are discussed in term of geometrical space model and with the help of the kinematical theory. It is shown that the small bundles produced by the CCVD technique are characterized by the presence of only a few helicities (one or two).

II. EXPERIMENT

The SWNT samples were synthesized on 2.5 wt % Co/MgO catalyst by decomposition of methane at 1000 °C and

purified by a hydrochloric acid treatment to remove the catalyst. The experimental procedure has been reported elsewhere.[9] Concerning the SWNT samples produced by electric arc discharge, they were synthesized with the mixture Ni/Y/C 0.5/0.5/99 at % following the procedure described in Ref. 8. In each case, the nanotube-containing material was mechanically transferred to a copper transmission electron microscope grid and examined in a JEOL 200 CX microscope.

III. GENERAL CONSIDERATIONS ON THE DIFFRACTION FROM SWNT BUNDLES

In the geometrical model of the reciprocal space of the nanotubes,[18–20] the presence of intensity in a given diffraction direction is related to a Bragg reflection of the flat graphite network suitably rolled up into a cylinder. The diffraction pattern is given by the intersection of the Ewald sphere with the distribution of nodes in reciprocal space and is shown to depend on the helicity and the tilt angle of the tube with respect to the incident electron beam.

The diffraction pattern of a bundle of SWNT's consists of intense spots along a line perpendicular to the needle axis, called the equatorial line, and a distribution of nonequatorial $hk.0$ nodes, elongated in the direction normal to the axis and having their intensity fading away towards the exterior. The spot positions along the equatorial line are determined by the stacking periodicity of the nanotubes and the orientation of the bundle of nanotubes with respect of the electron beam. The shapes and intensities of the spots depend on the size of the bundle and on the form factor of a single SWNT. This form factor can mainly be represented by a Bessel function of zero order, $rJ_0(Kr)$, which is the Fourier transform of a cylindrical objet of radius r, with K the scattering wave vector. Generally, the spots form streaks along the equatorial line axis, due to the strong curvature of the tubes and the finite size of the bundle, and the density of scattering is higher close to the origin.

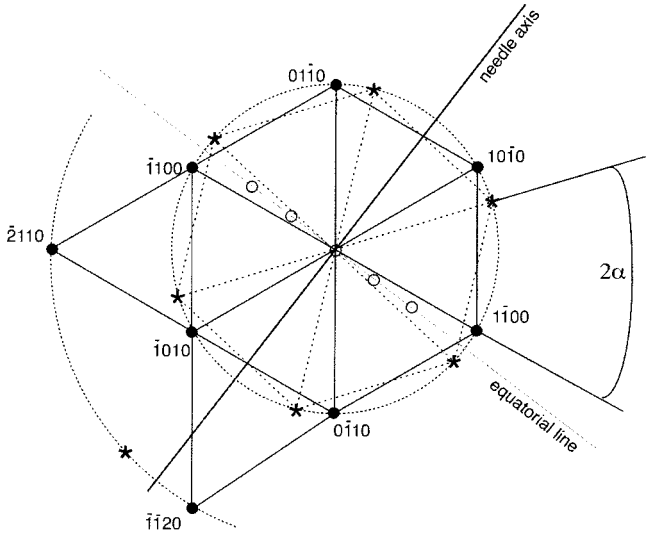

FIG. 1. Schematic diffraction pattern of a bundle made of chiral single-wall nanotubes with a unique helicity. The two hexagons of $10\bar{1}0$ graphitelike reflection (see text) are represented by two different symbols. They correspond to one another by a rotation of 180° about the nanotube axis. The open circles along the equatorial line sketch Bragg spots generated by the two-dimensional triangular lattice.

The other regions of high scattering density in reciprocal space correspond to the $hk.0$ reflections. The corresponding spots have a sharp end that originates from segments of the tubes which are normal to the incident electron beam. When the tube axis is normal to the incident electron beam, the hexagonal structure of the graphene layers causes a hexagonal arrangement of $10\bar{1}0$ and $11\bar{2}0$ reflections in the diffraction pattern. The orientation of this pattern depends on the helicity of the tube. For nonchiral nanotubes, the diffraction pattern exhibits a single hexagonal arrangement of reflection spots, whereas for chiral nanotubes each spot is split in two, and two sets of hexagons are observed. The angular separation between these hexagons is twice the chiral angle α of the tubes, which can thereby be determined. The complete pattern has still mm2 symmetry and is represented schematically in Fig. 1. Based on these geometrical considerations, the helicity can be estimated from the experimental electron diffraction patterns obtained at normal incidence. The value of α can be measured directly in the pattern from the relative positions of the spots around the first ($10\bar{1}0$ spots) or second ($11\bar{2}0$ spots) diffraction circles.

IV. RESULTS: OBSERVED DIFFRACTION PATTERNS

We now discuss a number of experimental diffraction patterns that were taken from isolated, straight bundle of SWNT's. As a first example, a typical diffraction pattern obtained with an isolated bundle of SWNT's produced by *electric arc discharge* is shown in Fig. 2. This bundle contains more than 50 nanotubes, perhaps as the result of the coales-

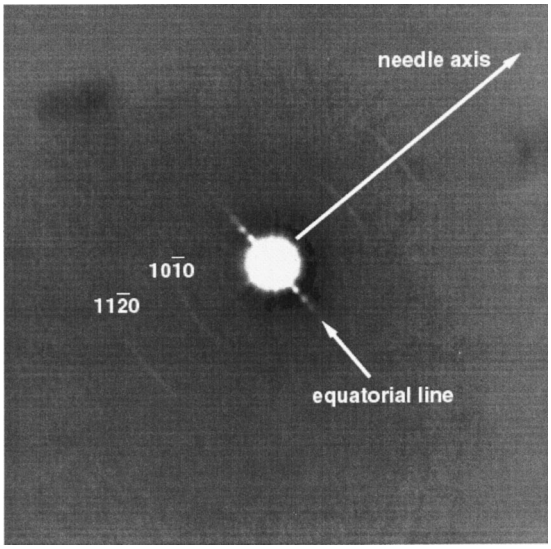

FIG. 2. Experimental selected-area electron diffraction pattern of a SWNT bundle synthesized by electric arc discharge.

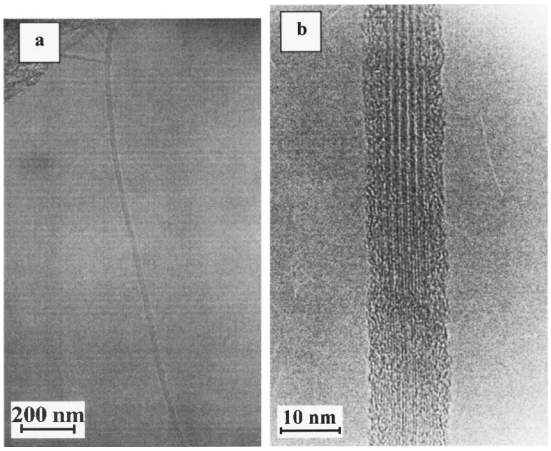

FIG. 3. (a) Low-magnification TEM image of an isolated straight SWNT bundle as the ones used in the ED experiments. (b) Higher-magnification image of the same bundle produced by CCVD, where the fringes related to lattice planes in Bragg conditions vary along the axis due to a twist.

cence of several smaller bundles.[25] Its diffraction pattern shows the two main features discussed here above: (1) a line of spots crossing the central 000 beam and perpendicular to the bundle axis (equatorial line) and (2) two diffuse arcs having their centers on the 000 beam. The radii of the inner and outer circles are consistent with the length of the diffraction vectors of type $10\bar{1}0$ and $11\bar{2}0$ of graphite, respectively. The diffracted intensity along the circles is neither spotty nor uniform over a complete ring. Instead, the largest intensity is found close to north and south poles, and a weaker one near the equator. This diffuse distribution of intensity is the indication of a random and continuous distribution of helicities.[25]

We now discuss the data obtained with SWNT's synthesized by the CCVD method and organized in nanobundles. The discussion proceeds in three steps: (1) the description of SWNT bundles from TEM images, (2) the helicity observed within the bundles, and (3) an analysis of the spot distribution along the equatorial line.

A typical example of an isolated straight bundle of SWNT's synthesized by the CCVD method is illustrated in Fig. 3. The bundles we selected for our diffraction experiment all have this aspect. Most of them were made of a small number of tubes because we tried to avoid polycrystalline bundles resulting from a grouping of several ropes. The size of the bundles studied is around 10 nm in diameter (20–30 tubes), which is much smaller than the size of the bundles considered in previous diffraction experiments. Moreover, as clearly seen in Fig. 3(b), the bundle presents different lattice fringe periods, which means different crystallographic orientations when moving along the axis. This modulation is due to the twist of the bundle[25] and, consequently, the electron beam in selected-area diffraction experiment probes various orientations of the crystal. From the HRTEM images, the lattice parameter can be estimated to be around 14 Å.

A first ED pattern obtained on a straight bundle is presented in Fig. 4(a). The $10\bar{1}0$ spots form two perfect hexagons on the inner circle and, also, $11\bar{2}0$ spots are observed close to the north and south poles on the second circle. This pattern suggests the presence of a single helicity, as discussed in the previous section. The diffraction pattern has the mm2 symmetry expected for a helical SWNT (see the previous section and Fig. 1). The angle 2α has been evaluated at around 48°; the chiral angle is therefore 24°. A precise measurement of the angle is made difficult by the streaking of the spots.

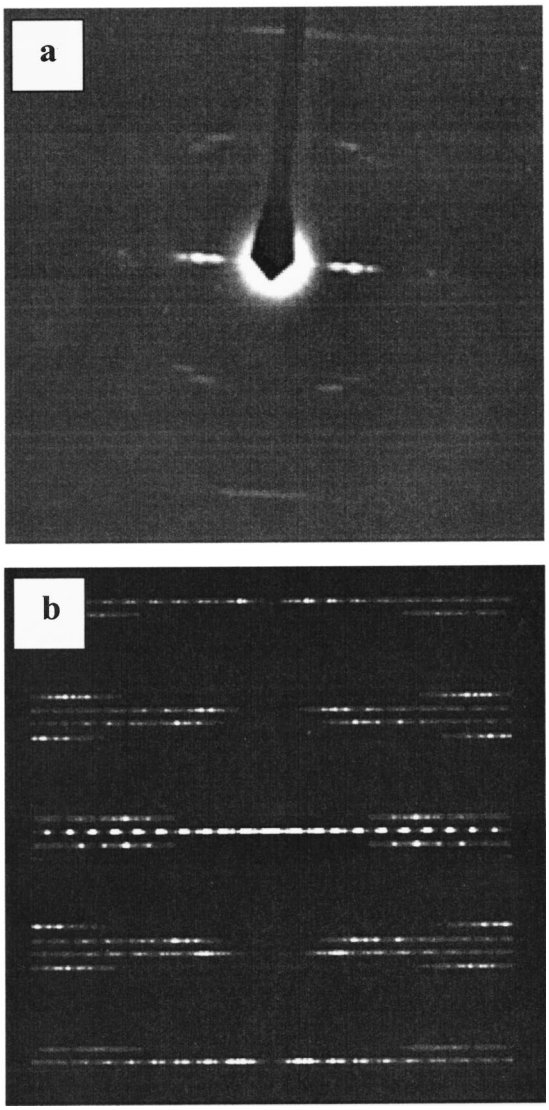

FIG. 4. Selected-area electron diffraction patterns of a SWNT bundle at normal incidence: (a) experimental and (b) simulated pattern computed for a bundle made of 31 (10,7) tubes with the kinematical theory.

Figure 4(b) shows a simulated diffraction pattern computed at normal incidence for an assembly of 31 (10,7) nanotubes on an triangular lattice. The calculated spot positions nicely fit the experimental diffraction pattern [Fig. 4(a)]. The (10,7) nanotubes have a diameter d_t of 11.6 Å and a chiral angle α of 24°. They were selected on the basis of the measured helicity and the approximate lattice parameter of 14 Å deduced by the HRTEM images, assuming a tube-tube dis-

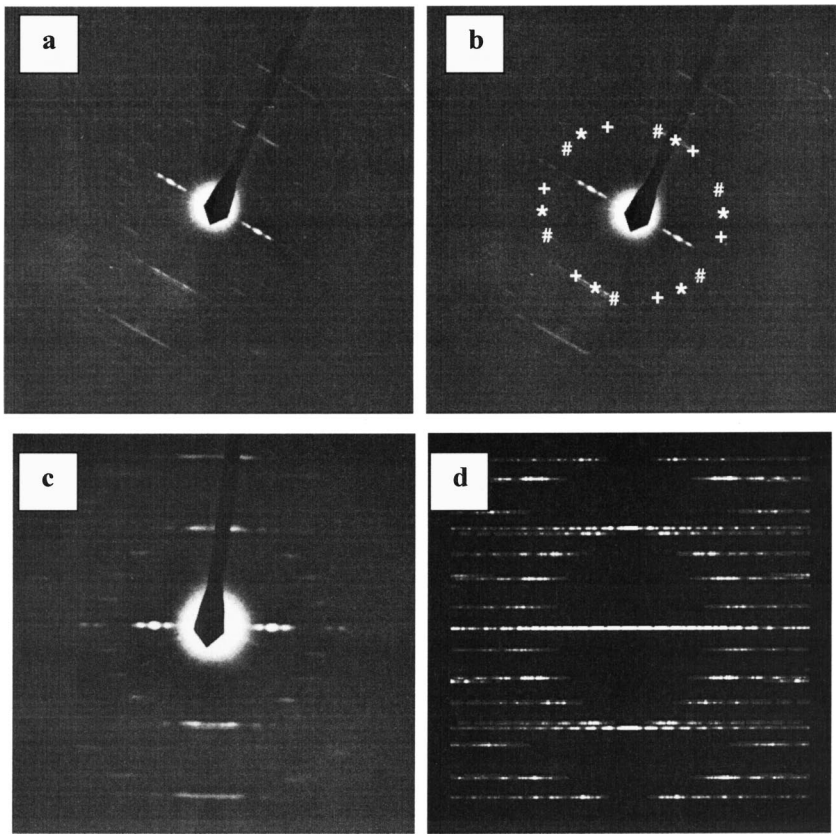

FIG. 5. Selected-area electron diffraction patterns of a SWNT bundle at normal incidence: (a) and (c) experimental patterns obtained with different exposure times, (b) experimental pattern with symbols identifying the three sets of hexagons, and (d) kinematical simulation for a bundle mixing a total of 31 (16,0) and (11,5) nanotubes.

tance of 3.2 Å. The value of the lattice parameter is confirmed by the analysis of the spot distributions along the equatorial line (see below). The others nanotubes with a chiral angle close to 24° are the (11,7) tubes ($d_t = 12.3$ Å, $\alpha = 23°$) and the (9,7) tube ($d_t = 10.9$ Å, $\alpha = 26°$), but their diameters do not agree so well with the experimental value.

A second diffraction pattern is shown in Fig. 5(a). The inner circle now contains three hexagons of weak, elongated spots identified with three different symbols in Fig. 5(b). The hexagon formed by the $10\bar{1}0$ spots, indicated by an asterisk *, corresponds to a zigzag structure. The other two sets of hexagons, denoted # and +, correspond to a chiral structure with an angle 2α estimated at around 32° and, then, correspond to a chiral angle of 16°. The planar symmetry of the diffraction pattern is again mm2. $11\bar{2}0$ spots with very weak intensities can also be observed on the outer circle, especially in Fig. 5(c). The differences between the two experimental diffraction patterns shown in Figs. 5(a) and 5(c) are the exposure times and the rotation of Fig. 5(c) that was performed to match the simulated pattern shown in Fig. 5(d). The simulated diffraction pattern was computed at normal incidence for an assembly of 31 nanotubes, in a bundle mixing (16,0) tubes ($d_t = 12.5$ Å, $\alpha = 0°$) and (11,5) tubes ($d_t = 11.1$ Å, $\alpha = 18°$). Another possibility leading to equivalent results is to mix (15,0) tubes ($d_t = 11.7$ Å, $\alpha = 0°$) with (12,5) tubes ($d_t = 11.8$ Å, $\alpha = 17°$).

The ED experimental patterns displayed in Figs. 4 and 5 are typical examples selected from a more systematic study. Well-defined diffraction patterns and corresponding HRTEM images have been recorded for a total of 20 bundles. The average diameter of the bundles considered in the ED experiments was around 10 nm. As already mentioned above, this diameter is much smaller than the one of bundles synthesized by the other production techniques. Here 45% of our diffraction patterns (nine) revealed a single helicity: one corresponding exactly to the armchair structure ($\alpha = 30°$) and the others (eight) to the chiral structures with helical angles close to 30° [exactly 21°, 23°, 24°, 25°, 26° (two), 28°, 29°]. We note that the helical angle values found in this study are close to 30°, but no preferred helicity came out. We observed bundles with two helicities in 40% of ED patterns like in Fig. 5. The helical angle values are in this case rather different (30°-20°, 16°-0°, 21°-28°, etc.). The last diffraction patterns exhibit several helicities (more than two), with the $10\bar{1}0$ circle, which appears, however, clearly spotty. When we considered bundles with larger diameters, the diffraction patterns obtained were found similar to the one shown in Fig. 2 for a large bundle synthesized by electric arc discharge.

We now discuss in details the intensity profile along the equatorial line. From the numerous diffraction patterns we have recorded, we observed that the equatorial line could be either clearly spotty or quite continuous. Several reasons can be put forward to explain the absence of well-defined spots. First, the crystalline order of the bundle might be poor. But the observation of well-defined fringes in HRTEM does not favor this argument. Second, the bundle might vibrate under the electron beam. We tried to minimize this effect by choosing bundles that were fixed at both ends. As a general rule, when we observed well-defined helicities in the diffraction pattern (such as in Figs. 4 and 5), the corresponding equato-

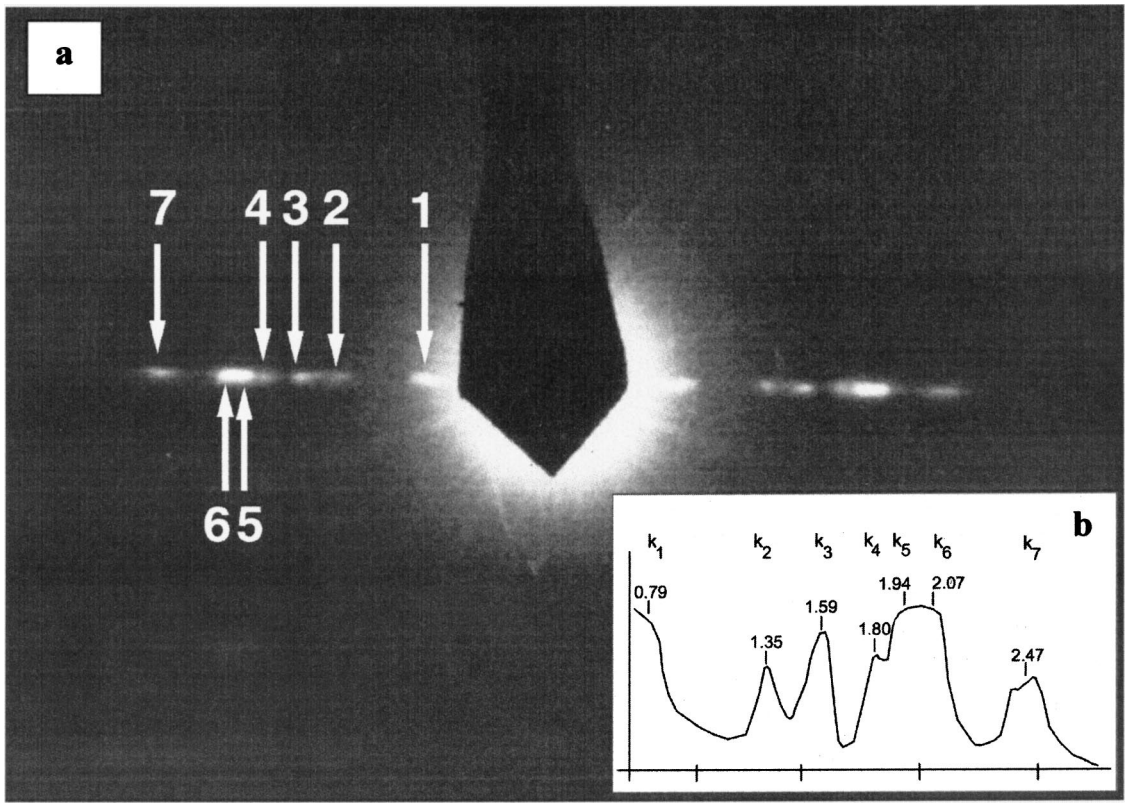

FIG. 6. (a) Magnification of the equatorial line of the SAED pattern of Fig. 5. Seven spots can be identified along this line. (b) Experimental equatorial line profile of intensities.

rial line presented well-defined spots as well. A typical example of a spotty equatorial line is shown in Fig. 6, which is the magnification of the equatorial line of the diffraction pattern of Fig. 5(a). Seven spots can be distinguished and, in spite of their elongated shape, their spacing can be measured to estimate the bundle lattice parameter.

Figure 7 represents three equatorial line profiles computed with the kinematical theory. The first two were computed for two homogeneous bundles corresponding to the two nanotubes mentioned before: (16,0) tubes ($d_t = 12.5$ Å) for the chiral angle of 0° and (11,5) tubes ($d_t = 11.1$ Å) for the chiral angle around 16°. The third profile is the sum of the first two curves that describes the diffraction pattern combining two nanobundles, one made of (11,5) tubes and the other made of (16,0) tubes. A bundle made of a random mixing of (11,5) and (16,0) tubes would present poorly defined peaks due to the disorder of the crystal. The widths of the peaks are the consequence of the finite number of tubes in the bundles and do not result from extra broadening. The helicity plays little role along the equatorial line of the diffraction pattern.

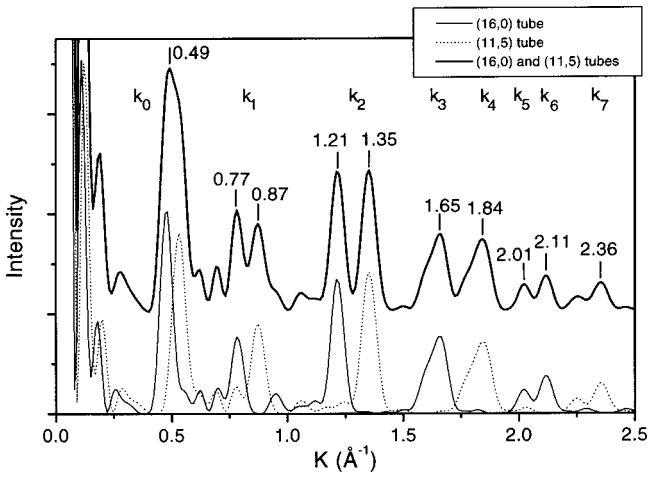

FIG. 7. Computed equatorial line profiles for SWNT bundles made of (16,0) and (11,5) nanotubes. The kinematical theory of diffraction within the continuum approximation has been used. An average over all rotation angles of the bundle around its axis was performed.

The comparison of the experimental diffraction profile and the simulated curve for (11,5) and (16,0) nanobundles (Fig. 7) indicates that the observed bundle could be the result of associating two monochiral nanobundles: one composed of nanotubes with chirality around 0° [(16,0) tubes] and another with chiral angle around 16° [(11,5) tubes]. It is also worth noting that the observed spot position can definitely not be attributed to a single crystal of SWNT's. This rules out the interpretation of the diffraction pattern as being due to a single crystal of SWNT's made of tubes with different helicities, but similar diameter.

For a further analysis, Table I lists the experimental values of the spots positions, as marked in Fig. 6(a), together with the positions of the Bragg reflections computed for *infinite* crystalline bundles with lattice parameter $a = 15.7$ Å (corresponding to a nanotube diameter of 12.5 Å, assuming

TABLE I. Comparison between the distances from the central beam of the equatorial spots (Fig. 6) and the positions of the Bragg reflections for two crystalline bundles with lattice parameter a and for the bundle mixing the two types of nanotubes (Fig. 7).

k	Experimental ($Å^{-1}$)	Theoretical ($Å^{-1}$)		Mixing	Bragg spots
		$a=15.7$ Å	$a=14.3$ Å		
1	0.79	0.800	0.872	0.82	(1,1)
2	1.35	1.222	1.342	1.28	(2,1)
3	1.59	1.600 1.666		1.65	(2,2) (3,1)
4	1.80		1.757 1.830	1.84	
5	1.94	2.014		2.01	(3,2)
6	2.07	2.117		2.11	(4,1)
7	2.47		2.325	2.36	

an intertube spacing of 3.2 Å) and 14.3 Å ($d_t=11.1$ Å). The small differences between the positions of the peaks indicated in Fig. 7 and the values given in Table I are due to the form factor of the tubes and the finite size of the bundles which Fig. 7 relates to. There is a reasonable correspondence between the experimental spot positions and the values given in Table I (named ''Mixing'') for the bundle mixing the two nanotubes with different diameter and helicity. In the simulation, the positions of the peaks k_1 and k_2 were taken at the center of the twin peaks in the third profile of Fig. 7. However we note that the position of the experimental spots is difficult to determine with precision due to their elongated shape. Each spot or couple of spots can then be associated with a Bragg reflection of one of the two nanocrystals.

Now, the relative intensities of the spot in the experimental spectrum [Fig. 6(b)] are not well reproduced by the computed line profile of Fig. 7, even if one takes into account the nonlinear response of the photographic film used to record the diffraction pattern. Part of the disagreement can be explained by the twist of the bundle, which continuously changes to the orientation of the bundle lattice with respect to the electron beam. In the calculations, an average on all possible orientations of the lattice was considered to simulate this effect. In order to reduce the range of possible orientations, the calculations were performed for a bundle having a six-fold symmetry, which is certainly not realistic. In addition, the twist of the bundle affects the form factor of the constituent nanotubes, since then the tubes spiral around the rope and are no longer straight as assumed here. A small change of form factor can modify the intensities of the Bragg spots. Finally, a deformation of the bundle could also change the relative intensities of the Bragg peaks.

V. DISCUSSION

A central question raised by the above data is to find an explanation for the monodispersity of chirality within a single SWNT bundle. This selectivity has already been mentioned in the literature,[7,26,31,32] but was never so clearly demonstrated.

First, we note that the samples studied in the present work were synthesized by the CCVD method, and no information about the helicity of SWNT's produced by that technique has been published so far. However, HRTEM studies and Raman spectroscopy indicate that the samples are composed of SWNT's organized in regular bundles, as well as isolated nanotubes. A complete description of the global morphology of the SWNT's produced by CCVD has been published elsewhere.[30] An important observation is that the diameter of the bundles is much smaller than the one of bundles synthesized by the other production techniques, perhaps because the catalytic particles on which the nanotube grow are smaller. In the 20 ED patterns analyzed in the present work, one (Fig. 4) or two (Fig. 5) tube helicities have been found in nine and eight small bundles, respectively. The fact that the spot features along the equatorial lines in Fig. 5 cannot been explained without invoking two distinct lattice periods and then two nanocrystals with different periodicity leads us to conclude that this bundle is an assembly of two nanobundles, each one being characterized by a *unique* diameter and helicity. It is then tempting to conclude that, in the initial stage of the formation, small bundles of SWNT's with a unique chirality are formed. The nanotube diameter of the samples considered in the present study is also smaller than the one commonly produced by the other synthesis techniques. A lattice parameter of 14 Å and a tube diameter around 11 Å were found, to be compared with the lattice parameter of 17 Å and tube diameter around 14 Å for commonly produced SWNT's.[7,8] However, the smaller diameter of such nanotubes is not the main reason for the strong selectivity of helicity, which is rather believed to be due to the small diameter of the bundles selected in the ED experiments. Larger bundles, as the ones produced by electric arc discharge or laser ablation, then appear as the result of the coalescence of smaller ones that have grown under slightly different conditions (temperature, composition, or orientation of the catalyst, etc.). This is why the electron diffraction pattern of such bundles revealed a large distribution of chiralities.

A last discussion concerns the chiral angles found experimentally when unique helicity is observed within a single bundle. In this case, the tube structures are close to armchair geometry. When two chiralities were observed, the helicity distribution seems to be broader. At this point, we do not know if these observations come from an intrinsic structural property of the nanotubes and then from a growth mechanism which would favor SWNT's close to armchair helicity.

VI. CONCLUSIONS

The diffraction patterns observed in the case of the SWNT bundle synthesized by the CCVD method show more chirality selectivity than the ones previously studied. The majority of the diffraction patterns of SWNT bundles clearly show the mm2 symmetry, with well-defined helicities and also a well-structured equatorial line. The chirality selectivity is explained by the small size of the bundles studied. We postulate that large bundles of SWNT's are an assembly of smaller, nanocrystalline ropes characterized by uniform helicities and diameters.

ACKNOWLEDGMENTS

The authors are grateful to the Belgian Inter-university Project on Reduced-Dimensionality Systems (PAI P4/10). L.H. is postdoctoral researcher at the FNRS. The authors also thank Professor J. B.Nagy (FUNDP, Namur) to have allowed the production of SWNT samples and Dr. C. Journet and Dr. P. Bernier (GDPC, Montpellier) for the SWNT sample synthesized by electric arc discharge.

*Corresponding author.
Electronic address: jfcolom@ruca.ua.ac.be

[1] S. Iijima, Nature (London) **354**, 56 (1991).
[2] M. M. J. Treacy, T. W. Ebbesen, and J. M. Gibson, Nature (London) **381**, 678 (1996).
[3] R. Saito, M. Fujita, G. Dresselhaus, and M. S. Dresselhaus, Appl. Phys. Lett. **60**, 2204 (1992).
[4] J. W. Minmire, B. I. Dunlap, and C. T. White, Phys. Rev. B **48**, 631 (1992).
[5] N. Hamada, S. I. Sawada, and A. Oshiyama, Phys. Rev. Lett. **68**, 1579 (1992).
[6] M. S. Dresselhaus, G. Dresselhaus, and P. C. Eklund, *Science of Fullerenes and Carbon Nanotubes* (Academic, New York, 1996).
[7] A. Thess, R. Lee, P. Nikolaev, H. Dai, P. Petit, J. Robert, C. Xu, Y. H. Lee, S. G. Kim, A. G. Rinzler, D. T. Colbert, G. E. Scuseria, D. Tomanek, J. E. Fisher, and R. E. Smalley, Science **273**, 483 (1996).
[8] C. Journet, W. K. Maser, P. Bernier, A. Loiseau, M. L. De La Chapelle, S. Lefrant, P. Deniart, R. Lee, and J. E. Fisher, Nature (London) **388**, 756 (1997).
[9] J.-F. Colomer, C. Stephan, S. Lefrant, G. Van Tendeloo, I. Willems, Z. Konya, A. Fonseca, Ch. Laurent, and J. B.Nagy, Chem. Phys. Lett. **317**, 83 (2000).
[10] S. Iijima and T. Ichihashi, Nature (London) **363**, 603 (1993).
[11] P. C. Eklund, J. M. Holden, and R. A. Jishi, Carbon **33**, 959 (1995).
[12] M. Lamy de la Chapelle, S. Lefrant, C. Journet, W. Maser, P. Bernier, and A. Loiseau, Carbon **36**, 705 (1998).
[13] S. Rols, R. Almairac, L. Henrard, E. Anglaret, and J.-L. Sauvajol, Eur. Phys. J. B **10**, 263 (1999).
[14] S. Bandow, S. Asaka, Y. Saito, A. M. Rao, L. Grigorian, E. Richter, and P. C. Eklund, Phys. Rev. Lett. **80**, 3779 (1998).
[15] M. Takizawa, S. Bandow, T. Torii, and S. Iijima, Chem. Phys. Lett. **302**, 146 (1999).
[16] C. Journet, Ph.D. thesis, University of Montpellier, 1998.
[17] L. Alvarez, T. Guillard, J. L. Sauvajol, G. Flamant, and D. Laplaze, Appl. Phys. A: Mater. Sci. Process. **70**, 169 (2000).
[18] X. B. Zhang, X. F. Zhang, S. Amelinckx, G. Van Tendeloo, and J. Van Landuyt, Ultramicroscopy **54**, 237 (1993).
[19] X. F. Zhang, X. B. Zhang, G. Van Tendeloo, S. Amelinckx, M. Op de Beek, and J. Van Landuyt, J. Cryst. Growth **130**, 368 (1993).
[20] S. Amelinckx, A. Lucas, and Ph. Lambin, Rep. Prog. Phys. **62**, 1471 (1999).
[21] L. C. Qin, J. Mater. Res. **9**, 2450 (1994).
[22] A. A. Lucas, V. Bruyninckx, and Ph. Lambin, Europhys. Lett. **35**, 355 (1996).
[23] Ph. Lambin and A. A. Lucas, Phys. Rev. B **56**, 3571 (1997).
[24] D. Bernaerts, A. Zettl, N. G. Chopra, A. Thess, and R. E. Smalley, Solid State Commun. **105**, 149 (1998).
[25] L. Henrard, A. Loiseau, C. Journet, and P. Bernier, Eur. Phys. J. B **13**, 661 (2000).
[26] J. M. Cowley, P. Nikolaev, A. Thess, and R. E. Smalley, Chem. Phys. Lett. **265**, 379 (1997).
[27] R. R. He, H. Z. Jin, J. Zhu, Y. J. Yan, and X. H. Chen, Chem. Phys. Lett. **298**, 170 (1998).
[28] H. Z. Jin, R. R. He, and J. Zhu, J. Electron Microsc. **48**, 339 (1999).
[29] J. M. Cowley and F. A. Sundell, Ultramicroscopy **68**, 1 (1997).
[30] J.-F. Colomer, J.-M. Benoit, C. Stephan, S. Lefrant, G. Van Tendeloo, and J. B.Nagy, Chem. Phys. Lett. (to be published).
[31] L.-C. Qin, S. Iijima, H. Kataura, Y. Maniwa, S. Suzuki, and Y. Achiba, Chem. Phys. Lett. **268**, 101 (1997).
[32] L.-C. Qin and S. Iijima, Chem. Phys. Lett. **269**, 65 (1997).